IR Spectroscopic Observation windows and Analysis for Environmental Issues: Application to CO_2

Mohamed Abdessamia Chakchouk[1,2], Pierre Richard Dahoo[3], Abdelkhalak El Hami[4], Azzedine Lakhlifi[5], Dalal Fadil[6], Wajih Gafsi[7], Mohamed Haddar[7]

[1] LMN, INSA de Rouen, Saint Etienne de Rouvray, 76800, France
[2] Ecole Nationale des Ingénieurs de Sfax, Tunisie
[3] Université Paris-Saclay; UVSQ, CNRS, LATMOS, 78290 Guyancourt, France
[4] LMN, INSA de Rouen, Saint Etienne de Rouvray, 76800, France
[5] Université de Franche-Comté, CNRS, Institut UTINAM, F-25000 Besançon, France
[6] MINOS, Department of Electronics Engineering, Universitat Rovira i Virgili, 43007 Tarragona, Spain
[7] LA2MP, Ecole Nationale des Ingénieurs de Sfax, Tunisie

[*]Corresponding authors: azzedine.lakhlifi@obs-besancon.fr, ORCID 0000-0003-2024-6529; pierre-richard.dahoo@latmos.ipsl.fr

Abstract

Understanding the phenomena that can occur in a given medium necessitates a clear grasp of its chemical composition. In this context, various techniques including infrared (IR) spectroscopy were developed. In this work, we determined the bond force constants of CO_2 molecule in gas phase state and trapped in a nanocage by applying group theory to the normal vibrational modes of the symmetric ($^{16}O^{12}C^{16}O$, 626) and the asymmetric ($^{16}O^{12}C^{18}O$, 628) CO_2 isotopic species. Wilson's force, *F* and inverse-mass, *G* matrices, were calculated for the CO_2 (626 and 628) species. The effect of Fermi resonances were included in the analysis. Results are given in terms of bond force constants for stretching and bending modes of CO_2 molecule trapped in nanocages of rare gas matrices and of clathrate hydrates. The comparison with the gas phase values demonstrated that the condensed phase effect can be constrained at the harmonic level. A database of vibrational frequencies can then be built from the calculated values with a pseudo-uncertainty range to enhance automatic analysis of observed data pertaining to CO_2 in an unknown media by IR sensors. The study of CO_2 trapped in nanocages using group theory to calculate force constants has received little theoretical consideration in previous works. Here, we provide an additional approach to evaluate the uncertainty measurement in IR spectroscopy. Similar outcomes should be achievable for other molecules, providing the possibility to improve spectroscopic IR observation and analysis from sensors specially designed for mobile sensing applications.

Keywords: IR spectroscopy; group theory; environmental issues; global warming; carbon dioxide CO_2 isotopes.

1 Introduction

Global warming and sustainable development have opened a field of research focusing on environmental observation on earth [1, 2] . Diverse technological breakthrough and innovative methodologies are developed to bring sensors in the closest proximity of the medium of interest as practiced for planet, atmospheres, comets, or satellites observation as for example with Mars Express and Venus Express spatial missions [3–7]. One of the main methods used for atmosphere characterization on earth or elsewhere, is the infrared (IR) spectroscopy. Research activities that were dealing with this technology are segmented in two main aspects, theoretical and experimental. Advances in theoretical methods suitable for calculations of IR spectra opened the pathway to modeling IR spectra for various molecules. In fact, IR spectroscopy exhibits simulation progresses in multiple directions. On several levels, vibrational spectroscopy has created a remarkable synergy with theoretical and computational chemistry [8-14]. On the one hand, computational chemistry provides interpretation of the observed spectra, while, on the other hand, experimental spectroscopy provides support. The spectrum of a molecular species can be reconstructed using models based on contact transformation as described in the following references [15, 18] and references cited therein. A deconvolution of the observed spectra is necessary prior to the analysis in terms of intensity, width and line center characterizing a line shape as in [15, 18] and references cited therein. The experimental studies are conducted with an appropriate laboratory using instrumental set-up to identify the IR fingerprint of molecules [4-6, 18, 19]. Depending on the environment in which the molecule is observed, in laboratory nanocage trap medium, in a hostile experimental environment as in planetary observation, condensed phase or polymers such as silicone gels [20, 21], the IR spectrum is distorted. Consequently, the correlation between the precision of the molecular system's reference geometry, its energy and force constants, provide useful feedback on the performance and usefulness of quantum chemical approaches. It is therefore mandatory to correctly assign the molecular species from the observed IR data using the appropriate theoretical models and to analyze efficiently for example the data collected for CO_2 in different media using adequate sensors [22–33].

The principal issue is the limit of quantum chemistry techniques and their applicability to larger molecules. This is especially important for NIR (near infrared) spectroscopy, where the emphasis is on complicated samples and anharmonic approaches are required. In contrast, precision for smaller molecules under favorable circumstances dissolved in a moderately inert solvent is sufficient for a full interpretation of experimental NIR spectra [19, 35]. On the other hand, the incorporation of a chemical matrix in the anharmonic simulation is practically infeasible due to the computational complexity of these approaches. Such a matrix would be illustrative of a complicated sample encountered in analytical IR spectroscopy applications [8-10, 19]. Achieving this objective would pave the way for direct support from computational chemistry in analytical vibrational spectroscopy applications. In this work, we will present the symmetry based on theoretical tools for the spectroscopic study of molecules that allow the identification of the IR windows to be selected for observation in the design of the apparatus as discussed in references [1, 4-6, 19-21]. The aim is to provide a method to implement artificial intelligence [34] processes by identifying molecules or functional groups from IR or Raman active vibrations, when they are subjected to environmental constraints or when trapped in nanocages such as porous media [31,32] or clathrate hydrates [33, 36–42], or to chemical species in a crystal from vibrational factor group analysis [43, 44].

In this work, the model's set-up derived from group theory methods using, as a case study, the CO_2 molecule which is constantly under study as it is involved in global warming phenomenon [45-50]. Two isotopes of carbon dioxide are chosen: the standard symmetric $^{16}O^{12}C^{16}O$ and the asymmetric $^{16}O^{12}C^{18}O$. Their symmetry groups are, $D_{\infty h}$ and $C_{\infty v}$ as infinite order. They are analyzed using two subgroups of finite order, D_{2h} and C_{2v}, to determine their Wilson's *F* and *G* matrices [51] that allow to analyze their IR or Raman active vibrations. Then, based on well-established contact transformation theory for rovibrational study of linear molecules, pertinent resonances such as the Fermi-Dennison (FD) present in linear molecules, is accounted to analyze the fundamental vibrational levels in terms of bond force constants rather than global normal coordinates force constants. The method described is applied to fundamental vibrations of

CO_2 as observed in gas phase, in matrix isolation spectroscopy or in clathrates. This work is an attempt to provide a method of extraction of information on a molecular species trapped in a condensed medium, beyond standard gas phase IR spectroscopic values already present in data bases such as Hitran, from bond force constants. It targets the right set of IR windows in the design of mobile devices equipped with embedded appropriate sensors, antennas, and the electronics to collect data in an environment of IR spectroscopic interest. The focus is on the identification of condensed phase matter, such a clathrate, graphite surfaces or other type of medium, from trapped molecules' IR signature, for which the well-known gas phase IR spectra are modified due to the electromagnetic field from the condensed medium. This paper is organized as follows: section 2 describes the model and the calculation method based on symmetry considerations; section 3 presents the form giving the *F* and *G* matrices; section 4 is dedicated to the numerical results of the calculated force constant values for gas phase and trapped species in a matrix nanocage and section 5 is devoted to discussion about the results comparing the values for different environment and conclusions.

2 Model and methods

In this section, we describe how to set-up a model from group theoretical methods using the CO_2 molecule involved in global warming phenomenon as a model example. Two isotopes of carbon dioxide, the standard symmetric one $^{16}O^{12}C^{16}O$ and the asymmetric $^{16}O^{12}C^{18}O$ are chosen. Their symmetry groups, $D_{\infty h}$ and $C_{\infty v}$ being of infinite order, they are analyzed using two subgroups of finite order, D_{2h} and C_{2v}, in order to determine their Wilson's force, *F* and inverse-mass, *G* matrices [51] that allow analysis of their IR or Raman active vibrations.

2.1 Vibrational symmetry and normal coordinates

The application of mathematical group theory based on the symmetry of a chemical species is a powerful tool to study the vibrations and rotations of molecules as shown in references [15-18, 51] and references cited therein. In fact, group theory is applied to build a mathematical model of the Hamiltonian operator of the molecule from its symmetry properties. To

determine the vibrational IR fingerprint of a molecule, it is necessary to solve the Schrodinger's eigenvalues equation

$$\boldsymbol{H}|\boldsymbol{\Psi_v}\rangle = \boldsymbol{E_v}|\boldsymbol{\Psi_v}\rangle \quad (1)$$

where *H* is the Hamiltonian operator of the molecule, sum of its kinetic energy operator *T* and its potential energy operator *V*. $|\boldsymbol{\Psi_v}\rangle$ and $\boldsymbol{E_v}$ are the eigenfunction and eigenvalue, respectively, labelled by the index *v* which represents the vibrational quantum numbers that describe the independent vibrational modes.

The potential energy is generally expressed in terms of coordinates that are the most suitable to diagonalize the Hamiltonian operator and hence obtain the vibrational frequencies of the molecule. They correspond to the range of real values that the operator spans. In the case where only the vibrational degrees of freedom are considered, it is necessary to perform the calculations in the frame of reference tied to the molecule by applying Eckart-Sayvetz's conditions. The potential energy of a molecule is at its minimum when the molecule is in its equilibrium configuration. By setting the origin of the energies at the equilibrium configuration, only terms of degree greater than or equal to 2 contribute to the vibration energy. At the harmonic level, corresponding to second order terms, it is possible to use the internal coordinates R_k of the atoms in the molecule, and write the harmonic potential energy operator in the following form

$$\boldsymbol{2V} = \sum_i \sum_j \left(\frac{\partial^2 V}{\partial R_i \partial R_j}\right)_0 \boldsymbol{R_i R_j} = \sum_i \sum_j \boldsymbol{F_{ij} R_i R_j} \quad \text{or} \quad \boldsymbol{2V} = \boldsymbol{R'FR} \quad (2)$$

For small displacements of the atoms about their equilibrium positions, the kinetic energy operator of the molecule can be expressed in a similar form such as

$$\boldsymbol{2T} = \sum_i \sum_j \boldsymbol{M_{ij} \dot{R}_i \dot{R}_j} \quad (3)$$

where the parameters M_{ij} represent functions of the atomic mass and the equilibrium geometry of the molecule. It is more convenient to express the kinetic energy in terms of the conjugate variables defined as

$$\boldsymbol{P_i} = \frac{\partial T}{\partial \dot{R}_i} = \sum_j \boldsymbol{M_{ij} \dot{R}_j} \quad (4)$$

Then, Eq. (3) becomes

$$\boldsymbol{2T = \sum_i \sum_j G_{ij} P_i P_j} \qquad \text{or} \qquad \boldsymbol{2T = P' G P} \tag{5}$$

$\sum_j G_{ij} M_{jk} = \delta_{ik}$ or $GM = I$ in matrix form.

The best method to derive these equations is to use the normal coordinates, because *T* and *V* are simultaneously expressed in a diagonal form in the harmonic approximation. Internal coordinates are defined as linear combinations of normal coordinates as follows

$$R_j = \sum_k L_{jk} Q_k \tag{6}$$

where *j* amount ranging from 1 to n, and $\boldsymbol{L_{jk} = \frac{\partial R_j}{\partial Q_k}}$.

This transformation leads to the following relationships $2V = \sum_k \lambda_k Q_k^2$ and $2T = \sum_k \dot{Q}_k^2$

For each coordinate Q_k, the k^{th} vibrational mode, the frequency $\boldsymbol{\omega_k}$ is given by $\boldsymbol{\lambda_k = 4\pi^2 c^2 \omega_k^2}$.

In matrix formulation, the corresponding expressions write as

$$R = LQ \tag{7}$$

$$2V = Q' \Lambda Q \tag{8}$$

$$2T = \dot{Q}' \dot{Q} \tag{9}$$

where Λ is a diagonal matrix, whose elements are the parameters λ_k.

Substituting Eq. (7) into Eqs. (2) and (3) and comparing with Eqs. (8) and (9), respectively, leads to the following equalities

$\Lambda = L' F L$ and $L' M L = I$.

By combining the last two equations, we obtain the following form:

$$FL = ML\Lambda \tag{10}$$

and multiplying by $G = M^{-1}$, leads to

$$GFL = L\Lambda \tag{11}$$

The determinants of the two last equations verify

$$\left|F - \lambda M\right| = 0 \tag{12}$$

$$\left|GF - \lambda I\right| = 0 \tag{13}$$

Finally, the problem of determining the normal coordinates reduces to the calculation of the determinants once given M_{ij} or G_{ij}.

The symmetry coordinates can then be used to simplify the calculation of the determinants because they are linear combinations of internal coordinates based on the symmetry properties of the molecule. These symmetry properties allow the decomposition of the matrices in block forms according to the symmetry properties of the molecule. The transformation of the internal coordinates to the symmetry ones can be achieved by the transformation matrix U, such that: $\boldsymbol{S = UR}$ and $\boldsymbol{2V = R'FR = S'\mathcal{F}S}$, with $\boldsymbol{\mathcal{F} = U'^{-1}FU^{-1}}$ and $\boldsymbol{S = L^S Q}$. It can be shown that the internal coordinates are related to the normal coordinates as follows

$$\boldsymbol{R = LQ = U^{-1}L^S Q = U'L^S Q} \tag{14}$$

It is then necessary to express cartesian displacements ΔP from equilibrium configuration geometry in terms of the internal coordinates. The cartesian coordinates are set by fixing a local frame on each nucleus labelled i such that its displacement is given by ($\Delta x_i = x_i - x_i^e$, $\Delta y_i = y_i - y_i^e$, $\Delta z_i = z_i - z_i^e$) and by applying Eckart-Sayvetz's conditions. Note that the components of R are nonlinear functions of such displacements and in matrix form expresses as $R = B\Delta P$, where B is a rectangular matrix which can be transformed in a square matrix by including the translational and rotational degrees of freedom in the frame of Eckart-Sayvetz's conditions.

2.2 Symmetry Group and symmetry coordinates of the CO_2 molecule

As given in [16], the symmetry group of the $^{16}O^{12}C^{16}O$ isotope is the $D_{\infty h}$ group, while that of the isotope $^{16}O^{12}C^{18}O$ is $C_{\infty v}$. The reducible representation Γ of a group G is the direct sum of irreducible representations Γ^{α} of the group such that

$$\Gamma = \boldsymbol{a_1\Gamma^1 \oplus a_2\Gamma^2 \oplus \ldots\ldots \oplus a_d\Gamma^d = \sum_{\oplus\alpha} a_\alpha \Gamma^\alpha} \quad (15)$$

when the number of irreducible representations is equal to d. The coefficients a_α, the number of times the irreducible representation Γ^α appears in the representation Γ are calculated from the following formula (Ref. [11] Eq. (1.23))

$$\boldsymbol{a_\alpha = \frac{1}{h}\sum_{O_i \epsilon G} h_i \chi(O_i)\left(\chi^\alpha(O_i)\right)^*} \quad (16)$$

where h is the order of the full symmetry group, O_i the one of the geometrical symmetry operations of the group, and χ^α is the trace of the matrix of the symmetry operation in the basis of the irreducible representation α of order h_i with

$$\boldsymbol{\chi(O_i) = \sum_\alpha a_\alpha \chi^\alpha(O_i)} \quad (17)$$

This expression is used to find the number of vibrations belonging to a given irreducible representation of the molecular point group from the various types of vibrations of a molecule which may be a single or degenerate stretching mode, bending mode, torsion mode, twisting mode or wagging mode. However, when h is infinite as for groups $D_{\infty h}$ and $C_{\infty v}$, the formula cannot be applied. Then, the corresponding sub-groups D_{2h} for $^{16}O^{12}C^{16}O$ and C_{2v} for $^{16}O^{12}C^{18}O$ are used instead. The correlations between the irreducible representations of the sub-groups and those of the full groups allow identification of the corresponding irreducible representations of the fundamental vibrations.

Following the method described in chapter 3 of Ref. [16], for the D_{2h} group of order $h = 8$, the reducible representation Γ writes:

$\Gamma = A_g + B_{1g} + B_{2g} + 2B_{1u} + 2B_{2u} + 2B_{3u}$, in terms of the irreducible representation of D_{2h}. For the translational and rotational degrees of freedom, the reduction writes

$\Gamma_{translation} = B_{1u} + B_{2u} + B_{3u}$ and $\Gamma_{rotation} = B_{1g} + B_{2g} + B_{3g}$. Note that as the molecule is linear, the B_{3g} term for the rotation movement vanishes. Consequently, for the vibrational degrees of freedom, $\Gamma_{vibration} = \Gamma - (\Gamma_{translation} + \Gamma_{rotation}) = A_g + B_{1u} + B_{2u} + B_{3u}$. The four vibrations hence determined correspond to two stretching modes and two bending ones. Similarly, in the case of the C_{2v} group of order $h = 4$, the reducible representation Γ writes

$\Gamma = 3A_1 + 3B_1 + 3B_2$, in terms of the irreducible representations of C_{2v}. For the translational and rotational degrees of freedom, the reduction writes

$\Gamma_{translation} = A_1 + B_1 + B_2$ and $\Gamma_{rotation} = A_2 + B_1 + B_2$. The molecule being linear, this time the A_2 term for rotation vanishes. Consequently, for the vibrational degrees of freedom, $\Gamma_{vibration} = \Gamma - (\Gamma_{translation} + \Gamma_{rotation}) = 2A_1 + B_1 + B_2$. The four vibrations hence determined also correspond to two stretching modes and two bending ones. The projection method, as applied in chapter 3 of [16], is used to determine the symmetry coordinates from the internal coordinates of the molecule, defined as the bond length between atoms 1 and 2 and atoms 2 and 3 of the linear CO_2 molecule and the angle between the two bonds in 2 perpendicular planes as shown in figure 1, for both isotopes $^{16}O^{12}C^{16}O$ and $^{16}O^{12}C^{18}O$. Then, atom 3 is ^{16}O for the symmetrical isotope and ^{18}O for the non-symmetrical one.

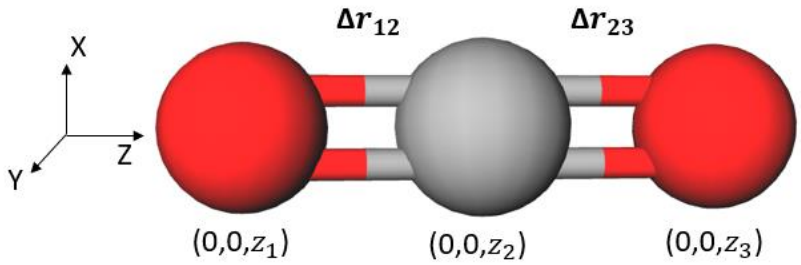

Figure 1. Internal and cartesian coordinates of the linear CO_2 molecule.

To determine the symmetries in terms of the irreducible representation, the projection formula is applied to the internal coordinates as shown in Ref. [16]

$$\boldsymbol{P^{\alpha}} = \frac{\boldsymbol{l_{\alpha}}}{\boldsymbol{h}} \sum_{\boldsymbol{O_i} \epsilon \boldsymbol{G}} \left(\boldsymbol{\chi^{\alpha}}\left(\boldsymbol{O_i}\right)\right)\boldsymbol{O_i} \tag{18}$$

For group D_{2h} for which $h = 8$, the applications of the symmetry operations on the internal coordinates are given in **table 1**. For the A_g irreducible representation, for example, $\boldsymbol{\chi^{A_g}}(\boldsymbol{O_i})$ is equal to 1 for all the symmetry operations of the group and $\boldsymbol{l_{A_g}}$ is equal to 1. In the case of the B_{1u} irreducible representation, $\boldsymbol{\chi^{B_{1u}}}(\boldsymbol{O_i})$ is equal to 1 or -1 depending on the symmetry operations and $\boldsymbol{l_{B_{1u}}}$ is equal to 1.

D_{2h}	E	$C_2(z)$	$C_2(y)$	$C_2(x)$	I	σ (xy)	σ (xz)	σ (yz)
Δr_{12}	Δr_{12}	Δr_{12}	Δr_{23}	Δr_{23}	Δr_{23}	Δr_{23}	Δr_{12}	Δr_{12}
Δr_{23}	Δr_{23}	Δr_{23}	Δr_{12}	Δr_{12}	Δr_{12}	Δr_{12}	Δr_{23}	Δr_{23}
$\Delta\alpha_1$	$\Delta\alpha_1$	$-\Delta\alpha_1$	$-\Delta\alpha_1$	$\Delta\alpha_1$	$-\Delta\alpha_1$	$\Delta\alpha_1$	$\Delta\alpha_1$	$-\Delta\alpha_1$
$\Delta\alpha_2$	$\Delta\alpha_2$	$-\Delta\alpha_2$	$\Delta\alpha_2$	$-\Delta\alpha_2$	$-\Delta\alpha_2$	$\Delta\alpha_2$	$-\Delta\alpha_2$	$\Delta\alpha_2$
A_{1g}	1	1	1	1	1	1	1	1
B_{1u}	1	1	-1	-1	-1	-1	1	1
B_{2u}	1	-1	1	-1	-1	1	-1	1
B_{3u}	1	-1	-1	1	-1	1	1	-1

D_{2h}	E	C_2 (z)	C_2 (y)	C_2 (x)	I	σ (xy)	σ (xz)	σ (yz)
Δr_{12}	Δr_{12}	Δr_{12}	Δr_{23}	Δr_{23}	Δr_{23}	Δr_{23}	Δr_{12}	Δr_{12}
Δr_{23}	Δr_{23}	Δr_{23}	Δr_{12}	Δr_{12}	Δr_{12}	Δr_{12}	Δr_{23}	Δr_{23}
Δa_1	Δa_1	$-\Delta a_1$	$-\Delta a_1$	Δa_1	$-\Delta a_1$	Δa_1	Δa_1	$-\Delta a_1$
Δa_2	Δa_2	$-\Delta a_2$	Δa_2	$-\Delta a_2$	$-\Delta a_2$	Δa_2	$-\Delta a_2$	Δa_2
A_{1g}	1	1	1	1	1	1	1	1
B_{1u}	1	1	-1	-1	-1	-1	1	1
B_{2u}	1	-1	1	-1	-1	1	-1	1
B_{3u}	1	-1	-1	1	-1	1	1	-1

Table 1. Table of vibrational irreducible characters representations of D_{2h} group

Applying the projection formula for the group D_{2h}, the corresponding symmetry coordinates are obtained for the stretching modes:

$$\boldsymbol{S_1^{A_g}} = \frac{1}{\sqrt{2}}\,(\Delta \boldsymbol{r_{12}} + \Delta \boldsymbol{r_{23}}) \tag{19a}$$

$$\boldsymbol{S_3^{B_{1u}}} = \frac{1}{\sqrt{2}}\,(\Delta \boldsymbol{r_{12}} - \Delta \boldsymbol{r_{23}}) \tag{19b}$$

and for the bending modes

$$\boldsymbol{S_{21}^{B_{3u}}} = \Delta\alpha_{\mathbf{1}} \tag{19c}$$

$$\boldsymbol{S_{22}^{B_{2u}}} = \Delta\alpha_{\mathbf{2}} \tag{19d}$$

For group C_{2v} for which $h = 4$, the applications of the symmetry operations on the internal coordinates are given in table 2. As shown for the A_1 irreducible representation, for example, $\boldsymbol{\chi^{A_1}}(\boldsymbol{O_i})$ is equal to 1 for all the symmetry operations of the group and $\boldsymbol{l_{A_1}}$ is equal to 1. In the case of the B_1 irreducible representation, $\boldsymbol{\chi^{B_1}}(\boldsymbol{O_i})$ is equal to 1 or -1 depending on the symmetry operations and $\boldsymbol{l_{B_1}}$ is equal to 1.

$\mathbf{C_{2v}}$	**E**	$\mathbf{C_2}$ **(z)**	σ **(xz)**	σ **(yz)**
$\mathbf{\Delta r_{12}}$	$\mathbf{\Delta r_{12}}$	$\mathbf{\Delta r_{23}}$	$\mathbf{\Delta r_{23}}$	$\mathbf{\Delta r_{12}}$
$\mathbf{\Delta r_{23}}$	$\mathbf{\Delta r_{23}}$	$\mathbf{\Delta r_{12}}$	$\mathbf{\Delta r_{12}}$	$\mathbf{\Delta r_{23}}$
$\mathbf{\Delta a_1}$	$\mathbf{\Delta a_1}$	$\mathbf{-\Delta a_1}$	$\mathbf{-\Delta a_1}$	$\mathbf{\Delta a_1}$
$\mathbf{\Delta a_2}$	$\mathbf{\Delta a_2}$	$\mathbf{-\Delta a_2}$	$\mathbf{\Delta a_2}$	$\mathbf{-\Delta a_2}$
$\mathbf{A_1}$	**1**	**1**	**1**	**1**
$\mathbf{B_1}$	**1**	**-1**	**1**	**-1**

$\mathbf{C_{2v}}$	**E**	$\mathbf{C_2(z)}$	**σ (xz)**	**σ (yz)**
$\mathbf{\Delta r_{12}}$	$\mathbf{\Delta r_{12}}$	$\mathbf{\Delta r_{23}}$	$\mathbf{\Delta r_{23}}$	$\mathbf{\Delta r_{12}}$
$\mathbf{\Delta r_{23}}$	$\mathbf{\Delta r_{23}}$	$\mathbf{\Delta r_{12}}$	$\mathbf{\Delta r_{12}}$	$\mathbf{\Delta r_{23}}$
$\mathbf{\Delta\alpha_1}$	$\mathbf{\Delta\alpha_1}$	$\mathbf{-\Delta\alpha_1}$	$\mathbf{-\Delta\alpha_1}$	$\mathbf{\Delta\alpha_1}$
$\mathbf{\Delta\alpha_2}$	$\mathbf{\Delta\alpha_2}$	$\mathbf{-\Delta\alpha_2}$	$\mathbf{\Delta\alpha_2}$	$\mathbf{-\Delta\alpha_2}$
$\mathbf{A_1}$	1	1	1	1
$\mathbf{B_1}$	1	-1	1	-1
$\mathbf{B_2}$	1	-1	-1	1

Table 2. Characters table of vibrational irreducible representations of C_{2v} group

Likewise, for group C_{2v}, the corresponding symmetry coordinates write as

$$\boldsymbol{S_1^{A_1}} = \frac{\mathbf{1}}{\sqrt{\mathbf{2}}}\,(\Delta \boldsymbol{r_{12}} + \Delta \boldsymbol{r_{23}}) \tag{20a}$$

$$\boldsymbol{S_3^{A_1}} = \frac{\mathbf{1}}{\sqrt{\mathbf{2}}}\,(\Delta \boldsymbol{r_{12}} - \Delta \boldsymbol{r_{23}}) \tag{20b}$$

$$\boldsymbol{S_{21}^{B_2}} = \Delta\alpha_{\mathbf{1}} \tag{20c}$$

$$\boldsymbol{S_{22}^{B_1}} = \Delta\alpha_{\mathbf{1}} \tag{20d}$$

For both symmetry group, the *U* matrix of Eq. (14) that gives *S* in terms of *R* through the relationship $S = UR$, writes

$$\boldsymbol{U} = \begin{bmatrix} \frac{\mathbf{1}}{\sqrt{\mathbf{2}}} & \frac{\mathbf{1}}{\sqrt{\mathbf{2}}} & \mathbf{0} & \mathbf{0} \\ \frac{\mathbf{1}}{\sqrt{\mathbf{2}}} & -\frac{\mathbf{1}}{\sqrt{\mathbf{2}}} & \mathbf{0} & \mathbf{0} \\ \mathbf{0} & \mathbf{0} & \mathbf{1} & \mathbf{0} \\ \mathbf{0} & \mathbf{0} & \mathbf{0} & \mathbf{1} \end{bmatrix} \tag{21}$$

when the *S* coordinates are arranged in the order S_1, S_3, S_{21} and S_{22} and the *R* coordinates are arranged in the order $\Delta \boldsymbol{r_{12}}$, $\Delta \boldsymbol{r_{23}}$, $\Delta\alpha_{\mathbf{1}}$ and $\Delta\alpha_{\mathbf{2}}$. Finally, from the correlation between the sub-groups and the full symmetry group, the following correspondences are determined for D_{2h} and $D_{\infty h}$ and C_{2v} and $C_{\infty v}$ as given in table 3.

D_{2h}	$D_{\infty h}$		C_{2v}	$C_{\infty v}$
A_g	Σ_g^+		A_1	Σ^+
B_{1u}	Σ_u^+		A_1	Σ^+
B_{2u}	π_u		B_1	π
B_{3u}			B_2	

Table 3. Correlation between IR of groups D_{2h} and $D_{\infty h}$ and of groups C_{2v} and $C_{\infty v}$

3 Wilson's *F* and *G* matrices

The expressions of the *GF* matrix in the basis of symmetry coordinates are calculated for the general XYZ form of a linear molecule which can also be applied to type XY_2. The potential energy function in terms of the internal coordinates is expressed as

$$\boldsymbol{V} = \boldsymbol{f_{11}}(\Delta \boldsymbol{r_{12}})^{\mathbf{2}} + \boldsymbol{f_{22}}(\Delta \boldsymbol{r_{23}})^{\mathbf{2}} + \mathbf{2}\boldsymbol{f_{12}}\Delta \boldsymbol{r_{12}}\Delta \boldsymbol{r_{23}} + \boldsymbol{f_{\alpha\alpha}}((\Delta \boldsymbol{\alpha_1})^{\mathbf{2}} + (\Delta \boldsymbol{\alpha_2})^{\mathbf{2}}) \tag{22a}$$

where f_{11}, f_{12}, f_{22} are the force constants associated with the vibrational stretching modes and $f_{\alpha\alpha}$ is the force constant associated with the vibrational bending mode. However, since the potential energy is invariant with respect to all the symmetry operations of the molecular point group, there are no cross terms of type $\Delta r_{ij}\Delta\alpha_k$ (i =1 or 2, j =2 or 3 and k =1 or 2). In terms of symmetry coordinates such that $F = UfU'$, where U' is the transpose of U, Eq. (22a) can be written as

$$V = F_{11}{S_1}^2 + F_{22}{S_3}^2 + 2F_{12}S_1S_3 + F_{\alpha\alpha}((S_{21})^2 + (S_{22})^2) \qquad (22b)$$

where F_{ii} and F_{ij} are respectively the diagonal and off-diagonal elements pertaining to the electro-mechanical force constants of the F matrix

$$\begin{bmatrix} \frac{1}{2}(f_{11}+f_{22}+2f_{12}) & \frac{1}{2}(f_{11}-f_{22}) & 0 & 0 \\ \frac{1}{2}(f_{11}-f_{22}) & \frac{1}{2}(f_{11}+f_{22}-2f_{12}) & 0 & 0 \\ 0 & 0 & f_{\alpha\alpha} & 0 \\ 0 & 0 & 0 & f_{\alpha\alpha} \end{bmatrix}. \qquad (22c)$$

The elements of the g matrix that involves the masses present in the kinetic energy operator term of the vibrational Hamiltonian, can be calculated following the method described in Ref. [51] from formula: $g_{tt'} = \sum_{k=1}^{3} \mu_k \vec{s}_{tk}\vec{s}_{t'k}$ where μ_k is the inverse of the mass of atom k and $\vec{s}_{tk}$ are the 3 unit vectors, one for each atom, such that they point in the direction that gives the maximum increase for internal coordinate R_t. For example, with the notation of Fig. 1

$$\vec{s}_{(\Delta r_{12})1} = \vec{e}_{21},\ \vec{s}_{(\Delta r_{12})2} = -\vec{e}_{21},\ \vec{s}_{(\Delta r_{12})3} = 0,\ \ \vec{s}_{(\Delta r_{23})1} = 0,\ \vec{s}_{(\Delta r_{23})2} = -\vec{e}_{23},$$

$$\vec{s}_{(\Delta r_{23})3} = \vec{e}_{23},\ \vec{s}_{(\Delta\alpha_1)1} = \frac{\vec{f}_{13}}{r_{12}},\ \vec{s}_{(\Delta\alpha_1)2} = -\left(\frac{\vec{f}_{13}}{r_{12}} + \frac{\vec{f}_{31}}{r_{23}}\right),\ \vec{s}_{(\Delta\alpha_1)3} = \frac{\vec{f}_{31}}{r_{23}}\ .$$

These expressions can be used to calculate the $\vec{s}_{tk}$ vectors such that:

$$\vec{s}_{11} = \frac{1}{\sqrt{2}}\vec{e}_{21}\,,\ \vec{s}_{12} = -\frac{1}{\sqrt{2}}(\vec{e}_{21}+\vec{e}_{23})\,,\ \vec{s}_{13} = \frac{1}{\sqrt{2}}\vec{e}_{23}\,,\quad \vec{s}_{21} = \frac{\vec{f}_{13}}{r_{12}},\ \vec{s}_{22} = -\left(\frac{\vec{f}_{13}}{r_{12}} + \frac{\vec{f}_{31}}{r_{23}}\right),$$
$$\vec{s}_{23} = \frac{\vec{f}_{31}}{r_{23}},\ \vec{s}_{31} = \frac{1}{\sqrt{2}}\vec{e}_{21}\ \ ,\vec{s}_{32} = -\frac{1}{\sqrt{2}}(\vec{e}_{21}-\vec{e}_{23})\ \ ,\vec{s}_{33} = -\frac{1}{\sqrt{2}}\vec{e}_{23}\ .$$

Then, for bond stretching and the 2 masses connected by bond Δr_{12}, g_{11} is given by

$$g_{11} = \frac{1}{m_1} + \frac{1}{m_2} \qquad (23a)$$

for bond stretching and the 2 masses connected by bond $\Delta \boldsymbol{r_{23}}$, $\boldsymbol{g_{22}}$ is given by

$$\boldsymbol{g_{22}} = \frac{\mathbf{1}}{\boldsymbol{m_2}} + \frac{\mathbf{1}}{\boldsymbol{m_3}} \tag{23b}$$

for bond stretching, with $\alpha = \pi$, the coupling term between bonds $\Delta \boldsymbol{r_{12}}$ and $\Delta \boldsymbol{r_{23}}$, $\boldsymbol{g_{12}}$ writes as

$$\boldsymbol{g_{12}} = -\frac{\mathbf{1}}{\boldsymbol{m_2}} \tag{23c}$$

and for inter-bond angle and the 2 masses connected by bonds $\Delta \boldsymbol{r_{12}}$ and $\Delta \boldsymbol{r_{23}}$, $\boldsymbol{g_{\alpha\alpha}}$ in each perpendicular plane is given by

$$\boldsymbol{g_{\alpha\alpha}} = \frac{\mathbf{1}}{\boldsymbol{r_{12}^2}}\frac{\mathbf{1}}{\boldsymbol{m_1}} + \frac{\mathbf{1}}{\boldsymbol{r_{23}^2}}\frac{\mathbf{1}}{\boldsymbol{m_3}} + \left(\frac{\mathbf{1}}{\boldsymbol{r_{12}^2}} + \frac{\mathbf{1}}{\boldsymbol{r_{23}^2}} + \frac{\mathbf{2}}{\boldsymbol{r_{12}r_{23}}}\right)\frac{\mathbf{1}}{\boldsymbol{m_2}} \tag{23d}$$

In terms of symmetry coordinates such that $G = UgU'$, the inverse-masses G matrix writes [25, 51]

$$\begin{bmatrix} \frac{1}{2}\left(\frac{1}{m_1}+\frac{1}{m_3}\right) & \frac{1}{2}\left(\frac{1}{m_1}-\frac{1}{m_3}\right) & 0 & 0 \\ \frac{1}{2}\left(\frac{1}{m_1}-\frac{1}{m_3}\right) & \frac{1}{2}\left(\frac{1}{m_1}+\frac{1}{m_3}+\frac{4}{m_2}\right) & 0 & 0 \\ 0 & 0 & \frac{1}{r_{12}^2}\frac{1}{m_1}+\frac{1}{r_{23}^2}\frac{1}{m_3}+\left(\frac{1}{r_{12}}+\frac{1}{r_{23}}\right)^2\frac{1}{m_2} & 0 \\ 0 & 0 & 0 & \frac{1}{r_{12}^2}\frac{1}{m_1}+\frac{1}{r_{23}^2}\frac{1}{m_3}+\left(\frac{1}{r_{12}}+\frac{1}{r_{23}}\right)^2\frac{1}{m_2} \end{bmatrix} \tag{24}$$

Finally, the GF matrix to be diagonalized can be written as [51]

$$\begin{bmatrix} \frac{1}{2}\left(\frac{f_{11}+f_{12}}{m_1}+\frac{f_{22}+f_{12}}{m_3}\right) & \frac{1}{2}\left(\frac{f_{11}-f_{12}}{m_1}-\frac{f_{22}-f_{12}}{m_3}\right) & 0 & 0 \\ \frac{1}{2}\left(\frac{f_{11}+f_{12}}{m_1}-\frac{f_{22}+f_{12}}{m_3}+2\frac{f_{11}-f_{22}}{m_2}\right) & \frac{1}{2}\left(\frac{f_{11}-f_{12}}{m_1}+\frac{f_{22}-f_{12}}{m_3}+2\frac{f_{11}+f_{22}-2f_{12}}{m_2}\right) & 0 & 0 \\ 0 & 0 & (GF)_{\alpha\alpha} & 0 \\ 0 & 0 & 0 & (GF)_{\alpha\alpha} \end{bmatrix} \tag{25}$$

in which $(\boldsymbol{GF})_{\boldsymbol{\alpha\alpha}} = \boldsymbol{f}_{\alpha\alpha}\left(\frac{\mathbf{1}}{\boldsymbol{r_{12}^2}}\frac{\mathbf{1}}{\boldsymbol{m_1}} + \frac{\mathbf{1}}{\boldsymbol{r_{23}^2}}\frac{\mathbf{1}}{\boldsymbol{m_3}} + \left(\frac{\mathbf{1}}{\boldsymbol{r_{12}}} + \frac{\mathbf{1}}{\boldsymbol{r_{23}}}\right)^2\frac{\mathbf{1}}{\boldsymbol{m_2}}\right)$.

Note, however, that *GF* can be separated in two matrices of 2 x 2 dimensions whose eigenvalues are the harmonic frequencies that are observed for the fundamental vibrations.

The eigenvalues $\boldsymbol{\lambda_1}$ and $\boldsymbol{\lambda_3}$ of the first 2 x 2 block matrix characterize the stretching symmetric and antisymmetric vibrational modes, they verify the conditions

$$\boldsymbol{\lambda_1\lambda_3} = \frac{\boldsymbol{m_1+m_2+m_3}}{\boldsymbol{m_1m_2m_3}}\left(\boldsymbol{f_{11}f_{22}} - \boldsymbol{f_{12}^2}\right) \tag{26a}$$

$$\boldsymbol{\lambda_1 + \lambda_3} = \left(\frac{\boldsymbol{1}}{\boldsymbol{m_1}} + \frac{\boldsymbol{1}}{\boldsymbol{m_2}}\right)\boldsymbol{f_{11}} + \left(\frac{\boldsymbol{1}}{\boldsymbol{m_2}} + \frac{\boldsymbol{1}}{\boldsymbol{m_3}}\right)\boldsymbol{f_{22}} - \frac{\boldsymbol{2}}{\boldsymbol{m_2}}\boldsymbol{f_{12}} \tag{26b}$$

In order to determine $\boldsymbol{f_{11}, f_{12}}$ **and** $\boldsymbol{f_{22}}$ force constants, Eq. (26b) is applied to the isotopic species (626) and (628) of CO_2 molecule, which leads to the following equation

$$\boldsymbol{\lambda_1 + \lambda_3 - \lambda'_1 - \lambda'_3} = \left(\frac{\boldsymbol{1}}{\boldsymbol{m_3}} - \frac{\boldsymbol{1}}{\boldsymbol{m'_3}}\right)\boldsymbol{f_{22}} \tag{26c}$$

for the end atom indexed 3 which is different in each isotopic species and from which f_{22} can be calculated.

Finally, $\boldsymbol{f_{\alpha\alpha}}$ can be calculated from the eigenvalue $\boldsymbol{\lambda_2}$ of the second block matrix and which is doubly degenerate and characterizes the bending vibrational mode given by

$$\boldsymbol{\lambda_2} = \boldsymbol{f_{\alpha\alpha}}\left(\frac{\boldsymbol{1}}{\boldsymbol{r_{12}^2}}\frac{\boldsymbol{1}}{\boldsymbol{m_1}} + \frac{\boldsymbol{1}}{\boldsymbol{r_{23}^2}}\frac{\boldsymbol{1}}{\boldsymbol{m_3}} + \left(\frac{\boldsymbol{1}}{\boldsymbol{r_{12}}} + \frac{\boldsymbol{1}}{\boldsymbol{r_{23}}}\right)^{\boldsymbol{2}}\frac{\boldsymbol{1}}{\boldsymbol{m_2}}\right) \tag{26d}$$

As the symmetric stretching mode ν_1 is in fermi resonance with the bending mode ν_2 when the latter absorbs 2 quanta of IR radiation, then two values are determined for $\boldsymbol{f_{11}}$ **and** $\boldsymbol{f_{12}}$ for each value of λ_1.

4 Numerical results

At the harmonic level, the observation of fundamental bands allows identification of the molecule from databases if the *GF* matrix is known from laboratory work. On the contrary, when the *GF* matrix is unknown, then, it can be determined if isotopic species are also present in the observed spectra because the *F* matrix does not depend on the atomic masses and provides unambiguous attribution. The theoretical approach is applied to carbon dioxide CO_2. In Section 4.1, the matrix *F* is calculated from the values of fundamental bands observed in matrices, for isotopes $^{16}O^{12}C^{16}O$ and $^{16}O^{12}C^{18}O$ [24-26].

4.1 Isotopes $^{16}O^{12}C^{16}O$ and $^{16}O^{12}C^{18}O$ in different media

The observed frequencies $\boldsymbol{\omega_k}$ (in wave numbers unit cm^{-1}) and the corresponding eigenvalues $\boldsymbol{\lambda_k}$(in s^{-2}) are related by the formula $\boldsymbol{\lambda_k = 4\pi^2 c^2 \omega_k^2}$, where *c* is the light velocity in vacuum. However when these frequencies are perturbed by resonances such as the Fermi-Dennison type, it is necessary to access to the unperturbed frequency value of the mode before calculating the bond force constant.

Thus, because the frequency of mode ν_1 is twice that of mode ν_2, then the quantum vibrational states labelled v_1 and v_2 such that $2\Delta v_1+\Delta v_2$ have the same values and where Δv_1 and Δv_2 are the changes in quantum numbers when a transition occurs between vibrational levels, the latter are subject to Fermi-Dennison (FD) resonance which splits the corresponding quasi-degenerate levels. The vibrational energy of these levels after the splitting of the quasi-degenerate levels are determined from the eigen values of a 2 x 2 matrix with diagonal terms given by the unperturbed frequency values of the absorbing modes and off-diagonal ones given by the FD resonance term [52]. If the energy of the unperturbed levels on the main diagonal of the matrix are noted E_a and E_b and the off-diagonal element, *W*, the characteristic equation of the 2 x 2 matrix leads to the following expressions from which the Fermi levels X_I and X_{II} can be obtained.

$$\boldsymbol{X_I = \frac{E_a+E_b}{2} + \sqrt{\left(\frac{E_a-E_b}{2}\right)^2 + W^2}} \quad (27a)$$

$$\boldsymbol{X_{II} = \frac{E_a+E_b}{2} - \sqrt{\left(\frac{E_a-E_b}{2}\right)^2 + W^2}} \quad (27b)$$

The unperturbed values can be determined by the inverse operation.

$$\boldsymbol{E_a = \frac{X_I+X_{II}}{2} + \sqrt{\left(\frac{X_I-X_{II}}{2}\right)^2 - W^2}} \quad (28a)$$

$$\boldsymbol{E_b = \frac{X_I+X_{II}}{2} - \sqrt{\left(\frac{X_I-X_{II}}{2}\right)^2 - W^2}} \quad (28b)$$

From the observed frequencies pertaining to the 626 ($^{16}O^{12}C^{16}O$) and 628 ($^{16}O^{12}C^{18}O$) isotopologues which were given in references [23-26] for gas phase and rare gas matrices and in references [23, 35, 36-40, 41] for structure I of the clathrate hydrate matrix, the corresponding

unperturbed values have been calculated for mode ν_1 and given in table 4 for the 626 ($^{16}O^{12}C^{16}O$) and 628 ($^{16}O^{12}C^{18}O$) isotopologues together with values observed for modes ν_2 **and** ν_3. From the corresponding eigenvalues λ_k(in s^{-2}), the bond force constants can then be calculated.

Isotope	Vibrational modes	Gas Phase	Argon Matrix	Krypton Matrix	Xenon Matrix	Clathrate hydrate I small cage	Clathrate hydrate I large cage
626	Stretching ν_1 calculated	1334.6	1330.8	1329.9	1329.3	1322.3	1328.1
626	Bending ν_2	667.4	661.9	660.6	659.3	655	660
626	Stretching ν_3	2349.2	2345.1	2340.6	2334.2	2347	2335
628	Stretching ν_1 calculated	1295.6	1291.8	1290.4	1289.2	1283.5	1285.7
628	Bending ν_2	662.4	656.8	656.1	655.2	650	655
628	Stretching ν_3	2332.1	2328.1	2323.9	2317.9	2330	2320

Table 4. Frequency values in wavenumbers (cm^{-1}) observed [23-26, 35, 38, 41, 52] for CO_2 isotopologues 626 and 628 in different media and calculated for mode ν_1.

4.2 Calculation of force constants for CO_2, in gas phase, rare gas matrices and clathrate hydrate I

From the following characteristic parameters, 1.162×10^{-10} m for the C-O bond length, 12.01074 $g.mol^{-1}$ for the mass of ^{12}C atom, 15.9994 $g.mol^{-1}$ and 17.9992 $g.mol^{-1}$ for ^{16}O and ^{18}O atoms, the values of the force constants can be determined from the formulas of Refs. [27] and [28] as given in table 5 for CO_2 in gas phase and trapped in rare gas matrices and in small and large cages of the structure I of clathrate. The effect of the electromagnetic field in the corresponding nanocage (trapping site in rare gas matrix or small cage or large cage in clathrate hydrate type I) is evaluated from the square of observed frequencies through the force constants.

Force constants	Gas phase	Argon Matrix	Krypton Matrix	Xenon Matrix	Clathrate hydrate I Small cage	Clathrate hydrate I Large cage
f_{11} (dyne/cm) x 10^{-5}	15.495	15.422	15.382	15.337	15.326	15.327
f_{12} (dyne/cm) x 10^{-5}	1.2963	1.2735	1.2886	1.3198	1.1557	1.3003
f_{22} (dyne/cm) x 10^{-5}	15.495	15.422	15.382	15.337	15.326	15.327
$f_{\alpha\alpha}$ (dyne.cm/rad^2) x 10^{12}	7.73626857	7.60928579	7.57942522	7.54962335	7.45146616	7.56566321

Table 5. Force constants for internal coordinates of CO_2 isotopologues 626 and 628 in different media

The force constants are fixed from the *L* matrix in Eq. (7), obtained from the eigenvectors of the *GF* matrix in terms of symmetry coordinates such that $\boldsymbol{L} = \boldsymbol{U}'\boldsymbol{L}^{\boldsymbol{S}}$, where the vector columns of $\boldsymbol{L}^{\boldsymbol{S}}$ are the eigenvectors of matrix *GF*. The $\boldsymbol{L}^{\boldsymbol{S}}$ matrix gives the normal coordinates Q_i in terms of the symmetric coordinates S_i. The fixed force constants are those that give Q_1 preferentially in terms of S_1 and Q_3 preferentially in terms of S_3.

5 Results and Discussion

The effect of the mechanical and electrical constraints imposed by the environment such as a nanocage in a condensed medium leads to a modification of the standard gas phase IR ro-vibrational spectra with the observation of an IR band structure either restricted to a Q branch in the absence of rotational degrees of freedom or to a perturbed P and R branches [9, 10, 12, 16, 20, 23-25, 36-40]. When a molecule moves in a constrained environment such as a nanocage, the external translational and rotational degrees of freedom are restricted and the electromagnetic field present in the nanocage in which the molecule is confined modifies the electronic potential that drives the motions of the nuclei resulting in a modification of the vibrational transitions. Specific theoretical models can be built to simulate the observed spectra [15-18, 26, 27, 33, 31, 53].

In rare gas matrices, the shifts increase from argon to xenon, being more important for the antisymmetric stretch than for the symmetric one and the bending mode. However, because there are 2 trapping sites in argon, a stable and an unstable one the shifts of the 3 modes are within the same range. The same trend is observed for the large cage and the small cage in clathrate hydrate type I. In the large cage results are similar for xenon. But in the small cage, the shifts of the symmetric stretch and bending modes are higher than in the large cage as given

in Table 4. As shown in sections 3 and 4, the bond force constants were calculated considering the correlations between the irreducible representations of the subgroups D_{2h} for $^{16}O^{12}C^{16}O$ and C_{2v} for $^{16}O^{12}C^{18}O$ and those of the full group $D_{\infty h}$ and $C_{\infty v}$, following the method described in references [16, 51] and in references cited therein, from the frequencies of the fundamental modes after a prior calculation of the frequency of the unperturbed ν_1 mode. The results obtained for mode ν_1 verify a significant progress in the analysis of CO_2 IR data from a result that was first shown and discussed by Amat and Pimbert [52]. These authors demonstrated that the frequency of the unperturbed ν_1 mode is at a lower value when compared to that of the $2\nu_2$ mode for the 626 isotopologue. It must be noted that it was the reverse situation that was then currently accepted. In this respect, our calculations show that likewise, the unperturbed ν_1 mode peaks at a lower value than the unperturbed $2\nu_2$ mode for both the 626 and 628 isotopologues when the molecule is trapped in a rare gas matrix or in a clathrate hydrate nanocage. To extract data pertaining to the latter environmental situation, the pertinent IR windows for observation must be located for the main absorption lines and the expected isotopologues.

Moreover, by applying the methods of quantum mechanics in the frame of contact transformations, the vibrational energy of a linear molecule can be expressed as

$$E_v = \sum_{s=1}^{3} \omega_s \left(v_s + \frac{g_s}{2}\right) + \sum_{s \le s'}^{3} x_{ss'} \left(v_s + \frac{g_s}{2}\right) \cdot \left(v_{s'} + \frac{g_{s'}}{2}\right) + \sum_{s \le s'}^{3} x_{\ell_s \ell_{s'}} \ell_s \ell_s \qquad (29)$$

where each normal mode of vibration of frequency $\boldsymbol{\omega_s}$ is labeled by the quantum number v_s and where $\boldsymbol{g_s}$ is the degree of degeneracy of the vibration ($\boldsymbol{g_s = 1}$ if not degenerate and $\boldsymbol{g_s = 2}$ if doubly degenerate) and the term with $\boldsymbol{\ell_s}$ which is related to the internal rotation of the degenerate vibration and which applies to the case of linear molecules. The anharmonic constants $\boldsymbol{x_{ss'}}$ and $\boldsymbol{x_{\ell_s \ell_{s'}}}$ are given by the perturbation calculation in the frame of contact transformation method and whose expressions are given in Refs. [16, 26] and references cited therein as well as the numerical values for linear symmetric and asymmetric CO_2 molecules.

To set IR observation windows for data collection and analysis, the initial step is to work on the bond force constants of the isolated molecule which is well known from theoretical works as presented in Refs. [11,12,15,16]. The method followed consists in defining a series of levels for the values of the bond force constants attributed to the isotopologues in free gas phase shown in sections 3 and 4. The first level is attributed to the most common isotopologue (626 for CO_2) and the other levels to the isotopologues in increasing order of masses of the atoms. This

corresponds to a change in the values of the elements of the *G* matrix. Then, following the simple rule that the square of the frequency is proportional to the force constant which is of electrical origin and inversely proportional to the mass which is of mechanical origin, the frequencies should scale down as the masses increase for the isotopologues.

Then, the second step is to define a series of levels when the molecule is confined in condensed media or on a surface. This time, because of the mean electromagnetic field to which the vibrating atoms are subjected, the bond force constants are modified for each isotopologue. In rare gas matrices, a red shift in band center is observed proportional to the polarizability of the rare gas atoms. But, in nitrogen matrix, a blue shift is observed instead for CO_2. Then, the shift may be either positive or negative depending on the condensed medium. This corresponds to a change in the values of the elements of the *F* matrix.

Therefore, for CO_2 molecule considered in this work, IR spectrum can be simulated from bond force constants that allow the calculation of normal mode of vibration of frequency $\boldsymbol{\omega_s}$ as shown in sections 3 and 4 from the *GF* matrix. Then, by applying the methods developed for Reliability Based Design Optimization (RBDO) [20, 54-56], based on a Monte-Carlo procedure, the IR windows to observe the fundamental $\boldsymbol{\nu_1}$, $\boldsymbol{\nu_2}$ and $\boldsymbol{\nu_3}$ bands can be simulated for isotopologues and for environments that differ from gas phase atmospheres, in particular nanocages that trap the molecule in condensed phase.

It can be observed from the results given in table 5, that the symmetry of the molecule is preserved since f_{11} and f_{22} are equal whatever the type of condensed matter trapping the CO_2 molecule in a nanocage. The maximum shifts of the force constants relative to gas phase values are equal to 1.09%, 1.81% and 3.68% respectively for $f_{11}= f_{22}$, f_{12} and $f_{\alpha\alpha}$. To compare, the relative shifts on the frequencies of the vibrational modes are respectively equal to 0.92%, 1.86% and 0.64% for the fundamental modes ν_1, ν_2 and ν_3.

In a first instance, the fundamental frequencies of the modes are calculated for the 628 isotopologue, from the calculated bond force constants of CO_2. The values compare well within less than 0.01% relative shifts for the three modes with observed values. Then, a Monte-Carlo procedure is applied to determine the frequencies by setting an uncertainty on the mass of one oxygen atom. Results show that the numerical procedure compares well with the analytical one in that the observed values lies within the calculated frequency intervals.

For the shifts observed in the nanocages with respect to the gas phase values, the MC procedure allows the determination of a window for observation which depends on the weight imposed on the value delivered by the random function. These weights have been set according to the relative shifts determined for the force constants calculated from observed values. The following distributions as shown in Fig. 2 are obtained for modes ν_1 and ν_3. The relationship being non-linear between the force constants and the calculated frequencies, the shape of the distributions is triangular. Note that for the ν_2 mode, this distribution of frequencies for MC run consisting of 10 000 steps, it is almost flat in the interval of calculated frequencies. These results reflect the relationship between the force constants and the calculated frequencies, since the ν_2 frequency scales as the square root of the force constant.

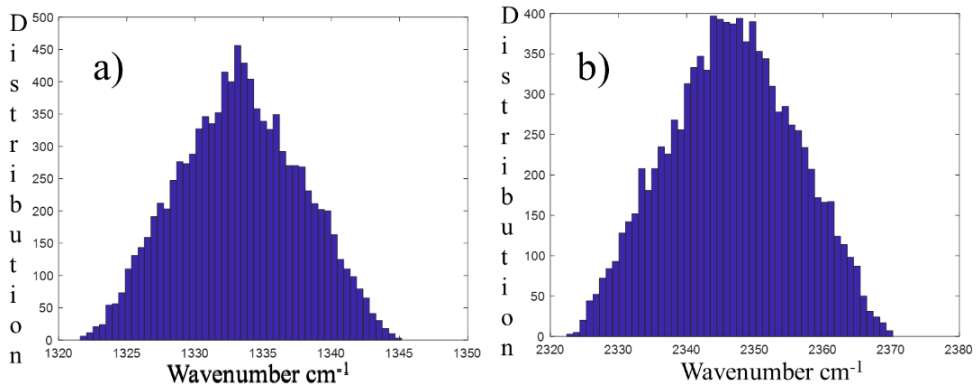

Figure 2. The distribution of frequencies for modes ν_1 (a) and ν_3 (b) for a set of weighted values given by the random function used for MC procedure with 10000 steps.

The association between the precision of the molecular system's reference geometry, its energy, and subsequently the bond force constants give valuable information regarding the performance and applicability of quantum physical and chemical techniques. The Monte-Carlo procedure is used to determine the range in which the bond force constants are expected when the molecule is trapped in a nanocage in a condensed matter environment. The fundamental frequencies are non-linear functions of the force constants. They are numerically obtained from the bond force constants determined from the MC procedure. Thus, as far as the internal vibrations are concerned, specific IR absorption windows can be localized for the analysis of data obtained from observed IR frequencies and different environments can be addressed from the analysis. For frequencies in resonance, a correction must be applied, such as the Fermi-Dennison one, to correct for the intervals.

In the design of a mobile detector, these specific windows can be optimized for in-situ analysis of data from any chemical species from IR or Raman spectroscopy. The mid infrared region which covers the IR domain from 400 cm^{-1} to 4000 cm^{-1}, is generally divided into four domains corresponding to: from 2500 cm^{-1} to 4000 cm^{-1} for O – H (3600 cm^{-1} to 3700 cm^{-1}), N – H (3300 cm^{-1} to 3400 cm^{-1}) and C – H (2850 cm^{-1} to 3000 cm^{-1}); from 2000 cm^{-1} to 2500 cm^{-1} for C ≡ C and C ≡ N; from 1500 cm^{-1} to 2000 cm^{-1} for C = C, C = O and C = N and from 600 cm^{-1} to 1500 cm^{-1} for C – C, C – O and C – N. These regions define the boundary limits to sense the IR transitions. Then, depending on environmental effects, these limits may fluctuate and accordingly be considered as IR domains subjected to uncertainties. To assess these uncertainties, the method described in this work can be applied.

Moreover, to account for the randomly generated character of the input parameters, the Monte-Carlo methods, in the frame of Reliability Based Design Optimization (RBDO) models [20, 54-56] can be coupled to Monte-Carlo Entropic Sampling (MCES) techniques [57-60] in order to enhance the effect of states beyond thermodynamic equilibrium in particular to account for temperature variations which impacts on the entropy of the molecular system under observation. Finally, the motivation behind the work presented lies in the application of RBDO and MCES techniques as numerical strategies to manage uncertainties such as those illustrated in this work.

Deep learning strategies applied in algorithm based on neural networks involves a training procedure from a great amount of data in order to determine the right weights on the different paths from the input to the output through the different layers considered in the algorithm. The rationale for starting with Monte Carlo techniques prior to delving into artificial intelligence (AI) lies in the need for a comprehensive and dependable database. Indeed, AI, specifically machine learning models, demonstrates optimal performance when provided with extensive and heterogeneous databases. In the initial steps, the range and distributions provided by the Monte Carlo procedure are used as training data for machine learning models. Thus, AI can easily from the trained algorithm extract data that are well known from experimental and theoretical work. So, in a first instance, one can let the algorithm identify what would have been obtained by conventional analysis from fitting of data to a model based on known data, and then work on those data that are left once conventional spectra of known molecular species have been identified.

The principal component analysis (PCA methods) coupled to Bayesian approach techniques are under considerations as methods to apply in order to analyze the then partially resolved observed data. Moreover, while our present emphasis is centered on carbon dioxide (CO_2) molecules, the fundamental ideas and approaches we have established, have wider relevance. The meticulousness and thoroughness of our Monte Carlo investigations, in conjunction with the potential of AI, provide a framework that may be extended to investigate further molecular systems.

A ro-vibrational gas phase molecular IR spectral line is generally characterized by its center, which is due to the transition between two quantum molecular levels induced by the operator involved in the transition (dipole moment, quadripolar moment, ..) , its half width at half maximum (HWHM) from Doppler effect and broadening by pressure leading to a shape described by a Voigt function, convolution of a Gaussian function with a Lorentzian one (in a first approximation narrowing of lines and other secondary effects may be neglected) and its surface area from the intensity which is due to Boltzmann statistics for the distribution of molecules on the energy levels and to spin statistics when similar nuclei can be interchanged in the molecule's equilibrium configuration.

Here we are addressing from the point of view of IR spectroscopy the identification of molecular species either well known because of their presence in the earth's atmosphere or because studied from theoretical models. There are thus 3 parameters to be determined from observed data which are provided in the true shape after correction of the apparatus function effect.

In gas phase, databases can provide the necessary data to train the AI algorithm to fit the line centers or peaks to those of known molecular species in gas phase. This allows identification of species in gas phase depending on the quality of the observed data and is quite straightforward. The identification of a molecule can be performed concurrently in different IR domains to analyze different ro-vibrational transitions (fundamental cold ones, combination bands, hot bands, …). Furthermore, depending on the IR range type of observed data, generally for MID IR between 400 cm^{-1} and 4000 cm^{-1}, it is necessary to consider simultaneously the different band centers from the lowest energy values (frequency or wavenumber values) that are fingerprints of the different possible isotopologues of the molecular species (for example CO_2).

6 Conclusion

In this work, we performed a simplified theoretical model based on group theory to determine the bond force constants for the CO_2 molecule in various media and predict an uncertainty interval to localize CO_2 in an otherwise unknown media. To the best our knowledge, it is the first time that calculations of the frequency attributed to the ν_1 mode for the unperturbed quantum vibrational state have been performed for CO_2 trapped in nanocages of rare gas matrices and clathrate of type I. The results are also in line with the results of Amat and Pimbert [52] about the relative position of the unperturbed quantum vibrational state ν_1 with respect to the $2\nu_2$ mode for the two isotopologues. A Monte Carlo procedure is then applied to vary either the bond force constants f_{ij} or the mass of the 3rd atom of CO_2 and the frequency interval in which to observe for the response of the molecule as an absorbent is determined. Then, the calculated corresponding vibrational frequencies can be optimized for every isotopologue to enlarge the database to analyze IR CO_2 observed data in condensed matter as well as the isotopic ratios. This work is an attempt to provide a method to extract information on a molecular species trapped in a condensed medium, beyond standard gas phase IR spectroscopic values already present in databases such as Hitran, from bond force constants. It provides a method to use Hitran data in order to select IR ranges to look for molecular species trapped in condensed matter in the design of mobile devices equipped with IR sensors. In this respect, the results of the present work may serve to analyze data expected from ESA large mission of exploration of the main satellites of Jupiter, the JUICE mission, since a lot of water is present on the planet's largest moons – Europa, Ganymede and Callisto buried under their icy surfaces [61]. In a next step, the method will be enlarged to the line shape, including the width and surface area besides the energy of the transition. The analysis of acquired data from IR spectroscopic instruments could further be enhanced by artificial intelligence tools resulting in significant simplification in the identification of chemical compounds.

Statements and Declarations

Competing Interests and Funding

The authors declare no conflict of interest.

No funding

Author Contributions

Conceptualization, P.R.D. and M.A.C.; methodology, P.R.D., A.L and M.A.C.; software, M.A.C. and A.E.H.; validation, P.R.D.; investigation, P.R.D. and A.L.; writing—original draft preparation, M.A.C., P.R.D., D.F. and A.E.H.; writing—review and editing, M.A.C., W.E.G., D.F. and M.H.; supervision M.A.C., W.E.G and M.H. funding acquisition, ‘no funding’. All authors have read and agreed to the published version of the manuscript.

Acknowledgments

This work was done in a collaboration between the LATMOS laboratory of the University of Versailles St-Quentin Paris-Saclay , and the UTINAM Institute of the University of Franche-Comté and the LMN laboratory of INSA Rouen Normandie in support by LA2MP laboratory of Sfax. Authors thank all of these institutions for their support. Special acknowledgement is dedicated to Dr. Hichame Maanane for the fruitful discussions.

Data Availability Statement: No Data associated in the manuscript".

References

[1] M. Meftah , L. Damé, P. Keckhut, S. Bekki, A. Sarkissian, A. Hauchecorne, E. Bertran, J.P. Carta, D. Rogers, S. Abbaki, X. Arrateig, C. Dufour, P. Gilbert, A.J. Vieau, L. Lapauw, N. Muscat, P. Bove, E. Sandana, F. Teherani, T. Li, G. Pradel, M. Mahé, C. Mercier, A. Paskeviciute, K. Segura, A. Berciano Alba, A. Aboulila, L. Chang, A. Chandran, P.R. Dahoo, A. Bui, Remote Sensing **12**, 24 (2020)

[2] M. Meftah, T. Boutéraon, C. Dufour, A. Hauchecorne, P. Keckhut, A. Finance, S. Bekki, S. Abbaki, E. Bertran, L. Damé, J.L. Engler, P. Galopeau, P. Gilbert, L. Lapauw, A. Sarkissian, A.J. Vieau, P. Lacroix, N. Caignard, X. Arrateig, O. D’Andon, A. Mangin, J.P. Carta, F. Boust, M. Mahé, C. Mercier, Remote Sensing **13**, 1449 (2021)

[3] J.L. Bertaux, O. Korablev, S. Perrier, E. Quémerais, F. Montmessin, F. Leblanc, S. Lebonnois, P. Rannou, F. Lefèvre, F. Forget, A. Fedorova, E. Dimarellis, A. Reberac, D. Fonteyn, J.Y. Chaufray, S. Guibert, J. Geophys. Research Planets **111**, E10S90 (2006)

[4] O. Korablev, J.L. Bertaux, A. Fedorova, D. Fonteyn, A. Stepanov, Y. Kalinnikov, A. Kiselev, A. Grigoriev, V. Jegoulev, S. Perrier, E. Dimarellis, J.P. Dubois, A. Reberac, E. Van Ransbeeck, B. Gondet, F. Montmessin, A. Rodin, J. Geophys. Research Planets **111**, E09S03 (2006).

[5] J.L. Bertaux , D. Nevejans, O. Korablev, E. Villard, E. Quémerais, E. Neefs, F. Montmessin, F. Leblanc, J.P. Dubois, E. Dimarellis, A. Hauchecorne, F. Lefèvre, P. Rannou, J.Y. Chaufray, M. Cabane, G. Cernogora, G. Souchon, F. Semelin, A. Reberac, E. Van Ransbeek, S. Berkenbosch, R. Clairquin, C. Muller, F. Forget, F. Hourdin, O. Talagrand, A. Rodin, A. Fedorova, A. Stepanov, I. Vinogradov, A. Kiselev, Yu. Kalinnikov, G. Durry, B. Sandel, A. Stern, J.C. Gérard, Planet Space Sci. **55**, 1673–1700 (2007)

[6] A. Mahieux, S. Berkenbosch, R. Clairquin, D. Fussen, N. Mateshvili, E. Neefs, D. Nevejans, B. Ristic, A.C. Vandaele, V. Wilquet, D. Belyaev, A. Fedorova, O. Korablev, E. Villard, F. Montmessin, J.L. Bertaux, Applied Optics **47**, 2252 (2008)

[7] J.L. Bertaux, A.C. Vandaele, V. Wilquet, F. Montmessin, R. Dahoo, E. Villard, O. Korablev, A. Fedorova, Icarus **195**, 28 (2008)

[8] K.B. Beć, J. Grabska, and C.W. Huck, Spectrochim. Acta A **254**, 119625 (2021)

[9] J. Grabska, NIR news. **32**, 7 (2021)

[10] G. Vasseur, Y. Fagot-Revurat, B. Kierren, M. Sicot, D. Malterre, Symmetry (Basel) **4**, 344 (2013)

[11] L. Han, F. Liu, L. Zhang, Symmetry (Basel) **13**, 1 (2021)

[12] R.E. Sonstrom, D.M. Cannon, J.L. Neill, Symmetry (Basel), **14**, 917 (2022)

[13] A. Cabrera-Ramirez, R. Prosmiti, J. Phys. Chem. C **126**, 14832 (2022)

[14] A. Cabrera-Ramirez, R. Prosmiti, J. Comput. Chem. **44**, 1587 (2023)

[15] P.R. Dahoo, A. Lakhlifi, Infrared Spectroscopy of Diatomics for Space Observation, (ISTE Ltd, London – John Wiley & Sons, Inc., Hoboken, 2017) vol. 1, pp. 210

[16] P.R. Dahoo, A. Lakhlifi, Infrared Spectroscopy of Triatomics for Space Observation, (ISTE Ltd, London – John Wiley & Sons, Inc., Hoboken, 2019) vol. 2, pp. 214

[17] P.R. Dahoo, A. Lakhlifi, Infrared Spectroscopy of Symmetric and Spherical Top Molecules for Space Observation 1, (ISTE Ltd, London – John Wiley & Sons, Inc., Hoboken, 2021) vol. 3, pp. 257

[18] P.R. Dahoo, A. Lakhlifi, Infrared Spectroscopy of Symmetric and Spherical Top Molecules for Space Observation 2, (ISTE Ltd, London – John Wiley & Sons, Inc., Hoboken, 2021) vol. 4, pp. 296

[19] T.G. Mayerhöfer, S. Pahlow, J. Popp, Spectrochim. Acta A **251**, 119411 (2021)

[20] P.R. Dahoo, P. Pougnet, A. El Hami, A Nanometer-scale Defect Detection Using Polarized Light, (ISTE Ltd, London – John Wiley & Sons, Inc., Hoboken, 2016) vol. 2, pp. 316

[21] P.R. Dahoo, P. Pougnet, A. El Hami, Applications and Metrology at Nanometer Scale 1: Smart Materials, Electromagnetic Waves and Uncertainties, (ISTE Ltd, London – John Wiley & Sons, Inc., Hoboken, 2021) vol. 9, pp. 246

[22] M. Margottin-Maclou, P.R. Dahoo, A. Henry, A. Valentin, L. Henry, J. Mol. Spectro. **131**, 21 (1988)

[23] F. Fleyfel, J.P. Devlin, J. Phys. Chem. **95**, 3811 (1995)

[24] V. Raducu, B. Gauthier-Roy, P.R. Dahoo, L. Abouaf-Marguin, J. Langlet, J. Caillet, M. Allavena, J. Chem. Phys. **105**, 10092 (1996)

[25] P.R. Dahoo, I. Berrodier, V. Raducu, J.L. Teffo, H. Chabbi, A. Lakhlifi, L. Abouaf-Marguin, Eur. Phys. J. D **5**, 71 (1999)

[26] A. Lakhlifi, H. Chabbi, P.R. Dahoo, J.L. Teffo, Eur. Phys. J. D **12**, 435 (2000)

[27] P.R. Dahoo, A. Lakhlifi, H. Chabbi, J.M. Coanga, J. Mol. Struct. **786**, 157 (2006)

[28] V. Wilquet, A. Mahieux, A.C. Vandaele, V.I. Perevalov, S.A. Tashkun, A. Fedorova, O. Korablev, F. Montmessin, R. Dahoo, J.-L. Bertaux, J. Quant. Spectrosc. Radiat. Transf. **109**, 895 (2008)

[29] G.L. Villanueva, M.J. Mumma, R.E. Novak, T. Hewagama, Icarus **195**, 34 (2008)

[30] M. Ghysels, G. Durry, N. Amarouche, Spectrochim. Acta A **107**, 55 (2013)

[31] C.Y. Chuah, W. Li, Y. Yang, T.H. Bae, Chem. Engineer. J. Adv. **3**, 100021 (2020)

[32] M. LI, A. Rojas Zuniga, P.L. Stanwix, Z.M. Aman, E.F. May, M.L. Johns, Fuel **312**, 122830 (2022)

[33] A. Lakhlifi, P.R. Dahoo, and E. Chassefière, J. Quant. Spectrosc. Radiat. Transf. **187**, 124 (2017)

[34] A. Argun, T. Thalheim, S. Bo, F. Cichos, G. Volpe, Applied Phys. Rev. **7**, 041404 (2020)

[35] S. Mayr, K.B. Beć, J. Grabska, V. Wiedemair, V. Pürgy, M.A. Popp, G.K. Bonn, C.W. Huck, Spectrochim. Acta A **249**, 119342 (2021)

[36] E. Dartois, B. Schmitt, Astron. Astrophys. **504**, 869 (2009)

[37] E. Dartois, M. Bouzit, B. Schmitt, EAS Publications Series **58**, 219 (2012)

[38] E. Dartois and F. Langlet, Astron. Astrophys. **652**, 869 (2021)

[39] E. Quirico, B. Schmitt, R. Bini, P.R. Salvi, Planetary and Space Science **44(9)**, 973 (1996)

[40] E. Quirico, B. Schmitt, Icarus **127(2)**, 354 (1997)

[41] J. Ghosh, R. Rajan, J. Methikkalam, R.G. Bhuin, G. Ragupathy, N. Choudhary, R. Kumar, T. Pradeep, Proc. Nat. Acad. Sci. **116**, 1526 (2019)

[42] P.S.R. Prasad, B.S. Kiran, Chem. Engineer. J. Adv. **3**, 100022 (2020)

[43] G. Bera, P. Mal, V.R. Reddy, U. Deshpande, P. Das, G. Padmaja, G.R. Turpu, Spectrochim. Acta A **227**, 117668 (2020)

[44] D. Haase, G. Hermann, J. Manz, V. Pohl, J.C. Tremblay, Symmetry (Basel) **13**, 205 (2021)

[45] Z.D. Reed, B.J. Drouin, D.A. Long, J.T. Hodges, J. Quant. Spectrosc. Radiat. Transf. **271**, 107681 (2021)

[46] M. Birk, C. Röske, G. Wagner, J. Quant. Spectrosc. Radiat. Transf. **272**, 107791 (2021)

[47] Z.D. Reed, B.J. Drouin, J.T. Hodges, J. Quant. Spectrosc. Radiat. Transf. **275**, 107885 (2021)

[48] I.E. Gordon, L.S. Rothman, R.J. Hargreaves, R. Hashemi, E.V. Karlovets, F.M. Skinner, E.K. Conway, C. Hill, R.V. Kochanov, Y. Tan, P. Wcisło, A.A. Finenko, K. Nelson, P.F. Bernath, M. Birk, V. Boudon, A. Campargue, K.V. Chance, A. Coustenis, B.J. Drouin, J.M. Flaud, R.R. Gamache, J.T. Hodges, D. Jacquemart, et al., J. Quant. Spectrosc. Radiat. Transf. **277**, 107949 (2022)

[49] D. Mondelain, A. Campargue, H. Fleurbaey, S. Kassi, S. Vasilchenko, J. Quant. Spectrosc. Radiat. Transf. **288**, 108267 (2022)

[50] D.A. Long, E.M. Adkins, J. Mendonca, S. Roche, J.T. Hodges, J. Quant. Spectrosc. Radiat. Transf. **291**, 108324 (2022)

[51] E.B. Wilson Jr., J.C. Decius, P.C. Cross, Molecular vibrations: the theory of infrared and Raman vibrational spectra, (McGraw-Hill, New York, 1955)

[52] G. Amat and M. Pimbert, J. Mol. Spectrosc. **16**, 278 (1965)

[53] I. Müller-Wodard, C.A. Griffith, E. Lellouch, T.E. Cravens, in Titan: Interior, Surface, Atmosphere, and Space Environment, (Cambridge University Press, Cambridge, 2014), pp. 29-62

[54] G. Kharmanda, M.H. Ibrahim, A. Abo Al kheer, F. Guerin, A. El Hami, Comput. Electron. Agric. **109**, 162 (2014)

[55] R. El Maani, A. Makhloufi, B. Radi, A. El Hami, Engineering Optimization **50**, 1715 (2018)

[56] P.R. Dahoo, P. Pougnet, A. El Hami, Applications and Metrology at Nanometer-Scale 2: Measurement Systems, Quantum Engineering and RBDO Method, (ISTE Ltd, London – John Wiley & Sons, Inc., Hoboken, 2021) vol. 10, pp. 274

[57] D. Chiruta, J. Linares, P.R. Dahoo, and M. Dimian, J. Applied Phys. **112**, 074906 (2012)

[58] D. Chiruta, C.M. Jureschi, J. Linares, P.R. Dahoo, Y. Garcia, and A. Rotaru, Eur. Phys. J. B **88**, 233 (2015)

[59] C. Cazelles, J. Linares, P.R. Dahoo, and K. Boukheddaden, Magnetochemistry **8**, 49 (2022)

[60] C. Cazelles, M. Ndiaye, P.R. Dahoo, J. Linares and K. Boukheddaden, Magnetochemistry **9**, 61 (2023)

[61] https://sci.esa.int/web/juice/publication-archive, https://www.esa.int/ESA_Multimedia/Images/2023/04/Juice_s_first_taste_of_science_from_space#.ZEvCniATwh0.link